Ionization of gases by a pulsed electron beam as studied by selffocusing. I. Monatomic gases

Hidehiko Arai and Hiroshi Hotta

Citation: The Journal of Chemical Physics **75**, 2252 (1981); doi: 10.1063/1.442285
View online: http://dx.doi.org/10.1063/1.442285
View Table of Contents: http://scitation.aip.org/content/aip/journal/jcp/75/5?ver=pdfcov
Published by the AIP Publishing

Ionization of gases by a pulsed electron beam as studied by self-focusing. I. Monatomic gases

Hidehiko Arai

Takasaki Radiation Chemistry Research Establishment, Japan Atomic Energy Research Institute, Takasaki, Gunma, 370-12 Japan

Hiroshi Hotta

Fukui Institute of Technology, Fukui, 910 Japan
(Received 4 February 1981; accepted 11 May 1981)

Ionization of He and Ar by a pulsed high-intensity electron beam from a Febetron 706 has been analyzed self-consistently with an electronic computer by using related data in references at pressures between 1 and 300 Torr. The computational results indicate that the net current I_{net} at pressures below 30 Torr of He and 10 Torr of Ar keeps a nearly constant value after a certain time which is comparable to the gas-breakdown time assumed previously. As the pressure is further increased, I_{net} increases gradually with time and E/p induced by the pulsed beam decreases with increasing pressure. Comparing the dose observed on the beam axis with the computational result has revealed that the increase of the dose in the higher pressure region is attributed to the increase of I_{net} due to the decreasing I_{back} induced by the pulsed beam. When the doses are compared at a certain pressure among monatomic gases, the larger dose is given by a gas with the larger mean ionization time t_i or $1/(\alpha w)$ for secondary ionization by E/p (α is the first Townsend ionization coefficient and w is the electron drift velocity). The data on self-focusing can be interpreted by this law.

INTRODUCTION

The self-focusing of a pulsed relativistic high-intensity electron beam from a Febetron 706 (tube 5515) has been analyzed in terms of a gas-breakdown time t_B in a previous paper[1] on the basis of the following model. Secondary electrons are pushed out of the beam channel till the space-charge neutralization time t_N. After t_N, the secondary electrons remaining in the beam channel are accelerated to the opposite direction against the beam coordinate z by an induced longitudinal electric field E_z. For the beam of a constant radius r_0 with a uniform electron density, E_z on the beam axis is given by

$$E_z = -\frac{2}{c^2}\left(\frac{1}{2}+\ln\frac{R}{r_0}\right)\frac{dI_{net}(t)}{dt} = c_1\frac{dI_{net}(t)}{dt}\ , \tag{1}$$

where R is the gas chamber radius, c is the light velocity, and the net current I_{net} is defined later. The production rate of secondary electrons can be expressed as

$$\frac{dn_e(t)}{dt} = \frac{n_0\sigma_{ion}(E_b)I_b(t)}{\pi e r_0^2} + \frac{n_e(t)}{t_i(t)}\ , \tag{2}$$

where n_e and n_0 are the number density of secondary electrons and neutral gas molecules respectively, $I_b(t)$ the beam current, and e the electron charge. The total ionization cross section σ_{ion} for beam electrons with energy E_b can be estimated with Rieke–Prepejchal's parameters[2]; E_b is assumed to be 480 keV as the mean energy[3] for the present beam. The mean ionization time t_i for secondary ionization by E_z can be estimated by

$$t_i = t_f/18.4 = 1/w(\alpha-\eta)\ , \tag{3}$$

where t_f is the breakdown formative time determined by Felsenthal and Proud,[4] w the electron drift velocity, α the first Townsend ionization coefficient, and η the electron-attachment coefficient. The plasma conductivity σ_e of the irradiated medium gas is given by

$$\sigma_e = \frac{e^2 n_e(t)}{n_0(2m)^{1/2}\langle Q_m(\epsilon)\epsilon^{1/2}\rangle}\ , \tag{4}$$

where m is the electron rest mass, and $Q_m(\epsilon)$ is the momentum transfer cross section to neutral molecules from electrons with kinetic energy ϵ.

In the previous paper,[1] in order to analyze the data without an electronic computer, it was assumed that the plasma backward current $I_{back}(t)$ is negligibly small till t_B, which is defined as the time when σ_e becomes 10 mho/cm, and that, after t_B, I_{net} given by

$$I_{net}(t) = I_b(t) + I_{back}(t) \tag{5}$$

keeps the nearly constant value which equals $I_b(t_B)$ because of increasing I_{back} with lapse of time. In Eq. (5), $I_{back}(t) < 0$ for $dI_{net}(t)/dt > 0$, from Eq. (1). On the other hand, the self-focusing of the pulsed beam has been measured as the dose on the beam axis at 10.4 cm from the chamber window by using a blue cellophane–aluminum piled dosimeter.[1] It has been found that the observed dose D_{obs} is approximately proportional to t_B in monatomic gases but the relationship between D_{obs} and t_B is not so simple in polyatomic gases as in monatomic gases.

In the present study, $I_{net}(t)$ in He and Ar is calculated self-consistently without the above assumption on $I_{net}(t)$ between t_N and t_B by using an electronic computer. The computation was carried out for the pulsed beam from a Febetron 706 according to the similar procedure with that made by McArthur and Poukey[5] and Swain,[6] although the present beam model is rather simplified than their model and the applied pressure region is more extensive than their one. Related values such as E_z, n_e, and σ_e are obtained in the course of the computation.

 0021-9606/81/172252-06$01.00

Kapchinskij and Vladimirskij[7] have given an equation for the beam envelope as

$$\frac{d^2 r_0}{dz^2} = \frac{A}{r_0} + \frac{\epsilon_b^2}{r_0^3} , \tag{6}$$

where the first term in the right side represents the self-focusing and the second the dispersion ($\pi\epsilon_b$: beam emittance). Since A is a quantity proportional to $I_{net}(t)$,[7,8] the envelope radius r_0 for the steady-state uniform beam ($d^2 r_0/dz^2 = 0$) is given by

$$r_0(t) = \epsilon_b/\sqrt{|A|} \propto \epsilon_b/\sqrt{I_{net}(t)} . \tag{7}$$

Therefore, if D_{obs} is assumed to be proportional to $I_b(t)/[\pi r_0(t)^2]$, we can obtain the equation

$$D_{obs} \propto \int \frac{I_b(t)\, I_{net}(t)}{\epsilon_b^2}\, dt \tag{8}$$

when t_N is short compared to the pulse duration.[8] The validity of the present value of I_{net} is demonstrated by comparing D_{obs} with the integral value in Eq. (8).

COMPUTATION FOR He AND Ar

In the present computation, $I_{net}(t)$ after t_N is assumed for Eq. (5) as

$$I_{net}(t) = I_b(t) + \pi r_0(t)^2 E_z(t)\, \sigma_e(t) . \tag{9}$$

For Eq. (4), the mean value of $Q_m(\epsilon)\epsilon^{1/2}$ is assumed as $\langle Q_m(\epsilon)\epsilon^{1/2}\rangle = Q_m(\bar{\epsilon})\bar{\epsilon}^{1/2}$, where $\bar{\epsilon}$ is the mean kinetic energy of secondary electrons. The beam profile $I_b(t)$ is assumed as shown by solid straight lines in Fig. 1. The beam radius r_0 is assumed to be 0.6 cm over the whole pulse duration. For $r_0 = 1.2$ cm, the value of $I_{net}(t)$ increased by about 20% at 10 and 50 Torr of Ar.

From Eqs. (1) and (9), $E_z(t+\Delta t)$ is given by

$$E_z(t+\Delta t) = c_1 \frac{I_b(t+\Delta t) - I_{net}(t)}{\Delta t - 2\pi c_1 r_0^2 \sigma_e(t+\Delta t)} . \tag{10}$$

The solution of Eq. (10) was obtained self-consistently referring to the Swain's paper.[6] In order to estimate $\sigma_e(t)$ with Eq. (4), $n_e(t)$ was computed by Eq. (2) with the Runge–Kutta method. Although the conductivity due to electron–ion collisions was added to Eq. (4), this contribution was not appreciable at least in the present pressure region. Furthermore, although the terms of dimer formation and electron–ion recombination were added to Eq. (2) as will be described in Part II, these effects were found to be negligibly small.

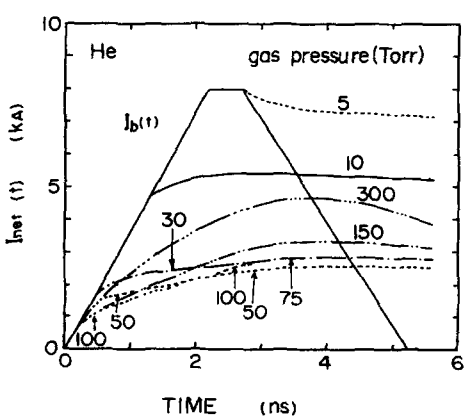

FIG. 1. The calculated net current $I_{net}(t)$ as a function of time for various pressures of He. The solid straight lines indicate the beam current $I_b(t)$.

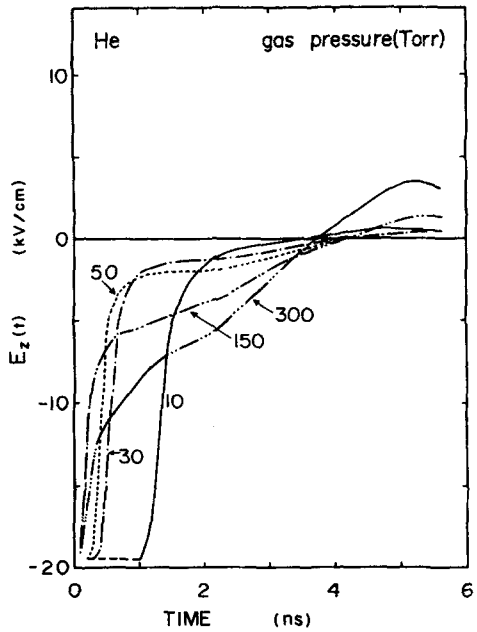

FIG. 2. The calculated induced longitudinal electric field $E_z(t)$ as a function of time for various pressures of He.

A. Computational results

1. He

The computation was carried out by using $\sigma_{ion}(480\ \text{keV}) = 1.98\times10^{-19}$ cm^2[2] and the known values for t_i,[4] D_L/μ[9] for $\bar{\epsilon}$ on the assumption of the Maxwellian, and $Q_m(\epsilon)$.[10] The results are shown in the following figures. Curves of $I_{net}(t)$ are shown in Fig. 1. The curve indicates that, up to 30 Torr at which D_{obs} is the minimum, $I_{net}(t)$ is approximately constant after a certain time so as to be able to determine the definite value of t_B^1 and that, at higher pressure, $I_{net}(t)$ increases gradually with the lapse of time. The corresponding E_z is shown in Fig. 2. Curves of $n_e(t)$ are shown in Fig. 3. The plateau value of $n_e(t)$ increases with increasing pressure up to 150 Torr at which $n_e(t) = 2.5\times10^{15}$ cm^{-3} and does not vary appreciably at higher pressure. The corresponding σ_e is shown in Fig. 4. The value becomes the maximum at near 30 Torr at which D_{obs} becomes the minimum. Values of $\bar{\epsilon}$ estimated from data on D_L/μ in the present E/p region are above 12 eV till at least 2 ns, irrespective of pressure.

2. Ar

The computation was carried out by using $\sigma_{ion}(480\ \text{keV}) = 9.99\times10^{-19}$ cm^2[2] and the known values for t_i,[4] D_L/μ,[9] and $Q_m(\epsilon)$.[10] The results are shown in Fig. 5 for $I_{net}(t)$, in Fig. 6 for $E_z(t)$, in Fig. 7 for $n_e(t)$, and in Fig. 8 for $\sigma_e(t)$. The curve of $I_{net}(t)$ up to 10 Torr varies in a way expected from the t_B model. The t_B model is not applicable in the pressure region in which

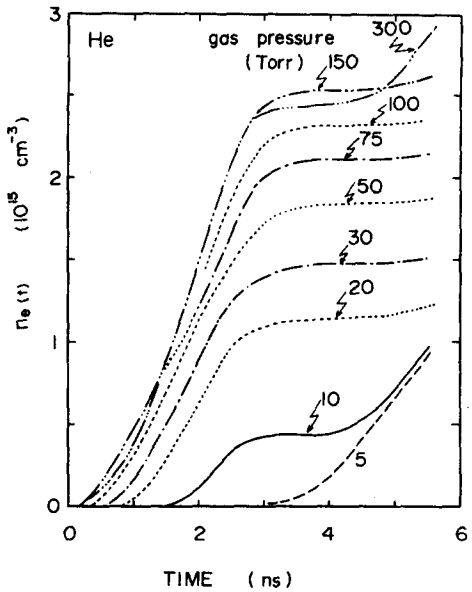

FIG. 3. The calculated number density $n_e(t)$ of produced secondary electrons as a function of time for various pressures of He.

D_{obs} increases gradually with increasing pressure. The plateau value of $n_e(t)$ increases up to 80 Torr with increasing pressure and decreases slightly with further increasing pressure. The maximum value is about 3×10^{15} cm^{-3}. The value of σ_e becomes the maximum at 10 Torr to be 5–6 mho/cm. Values of $\bar{\epsilon}$ estimated as for He are between 9 and 11 eV over the whole pressure range.

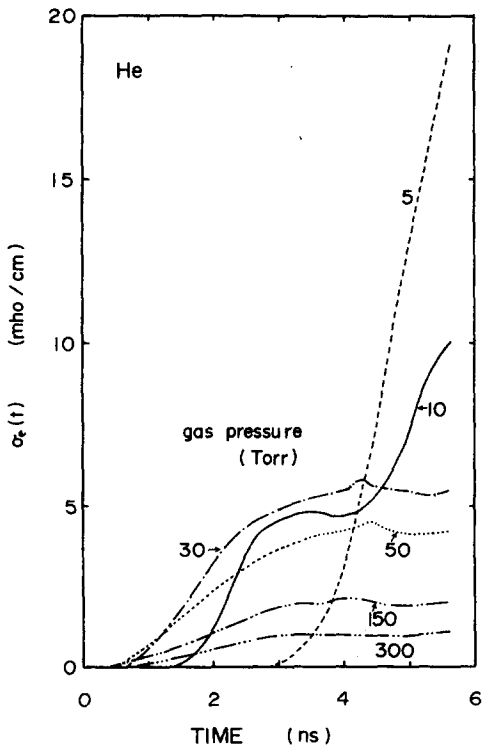

FIG. 4. The calculated plasma conductivity $\sigma_e(t)$ as a function of time for various pressures of He.

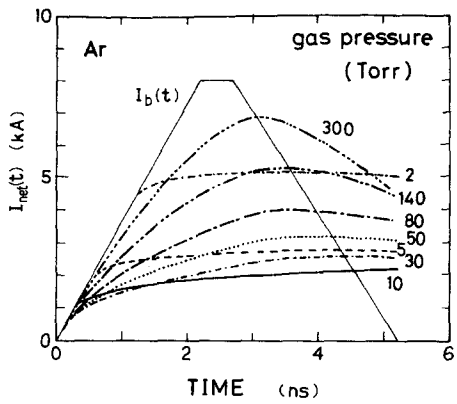

FIG. 5. The calculated net current $I_{net}(t)$ as a function of time for various pressures of Ar. The solid straight lines indicate the beam current.

B. Comparison with data on D_{obs}

Data on D_{obs} (the maximum dose of the depth–dose curve in the piled dosimeter) in monatomic gases[1] are plotted as functions of pressure in Fig. 9. Since the value of $\int I_b(t)\, I_{net}(t)\, dt$ may be proportional to D_{obs} from Eq. (8), values of the integral calculated from I_{net} in Figs. 1 and 5 are also plotted in an arbitrary unit by solid marks in Fig. 9. The calculated integral values for Ar corresponds well to the curve of D_{obs}, while such values for He have a minimum at 50 Torr in contrast with the minimum for D_{obs} at 20 Torr. The discrepancy for He may be due to ignorance of ionization of secondary electrons escaping radially as pointed out as the enhancement factor by McArthur and Poukey.[5] Decreasing of D_{obs} for Ar above 150 Torr is due to multiple scattering of the primary beam.

The minimum value of the integral is large for both gases in comparison with their minimum D_{obs}. This

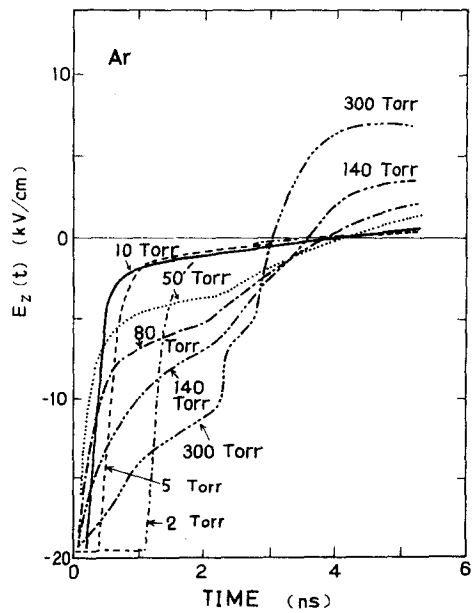

FIG. 6. The calculated induced longitudinal electric field $E_z(t)$ as a function of time for various pressures of Ar.

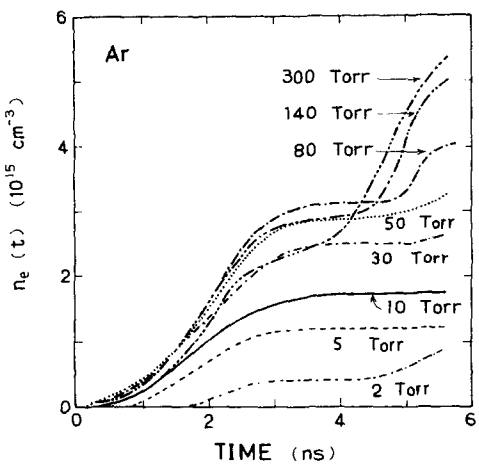

FIG. 7. The calculated number density $n_e(t)$ of produced secondary electrons as a function of time for various pressures of Ar.

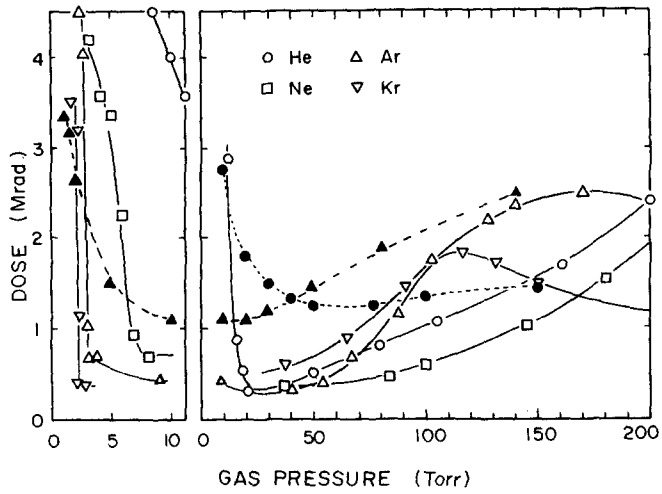

FIG. 9. D_{obs} at various pressures of monatomic gases; o (He), □ (Ne), Δ (Ar), and ▽ (Kr). Solid marks [● (He) and ▲ (Ar)] indicate the values of the integral in Eq. (9) in an arbitrary unit.

discrepancy is mainly attributed to variation of ϵ_b in Eq. (8) with D_{obs} because ϵ_b should be larger for the defocused beam than for the self-focused. Furthermore, when the envelope of the defocused beam is conical at the observing position (10.4 cm from a chamber window), the factor A in Eq. (6) should be smaller for the more defocused beam. Thus, when the correct values are used for A and ϵ_b, the curve of the integral may be fitted to that of D_{obs}. Consequently, D_{obs} is concluded to increase with increasing I_{net} as predicted by Eq. (8).

DISCUSSION

We can conclude from the present analysis that the gradual increase of D_{obs} with pressure above 10 Torr is attributed to the increase of I_{net} or the decrease of I_{back} in Eq. (10) because $I_{back} < 0$ for $dI_{net}(t)/dt > 0$. The value of I_{back} is determined by $\sigma_e E_z$. In Eq. (4), values of $Q_m(\bar{\epsilon})\bar{\epsilon}^{1/2}$ are nearly constant and equal to 1×10^{-15} cm^{2}eV$^{0.5}$ for $\bar{\epsilon} > 6$ eV in He and 8×10^{-15} cm^{2}eV$^{0.5}$ for 9–11 eV in Ar,[10,11] respectively. Furthermore, the time profile of $n_e(t)$ is almost the same till 2 ns at pressures above 100 Torr of He and 80 Torr of Ar. Then, $\sigma_e E_z$ becomes approximately proportional to E_z/p in such regions in which D_{obs} is higher than 1 Mrad. Curves of E_z/p from Figs. 2 and 6 are shown in Figs. 10 and 11 for He and Ar, respectively. These curves show that E_z/p decreases with increasing pressure more

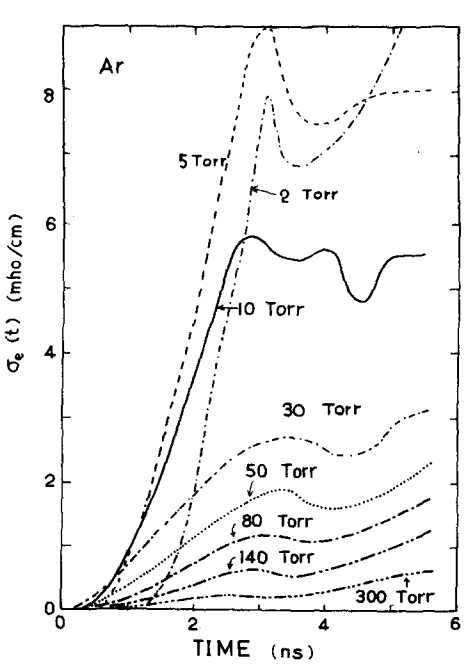

FIG. 8. The calculated plasma conductivity $\sigma_e(t)$ as a function of time for various pressures of Ar.

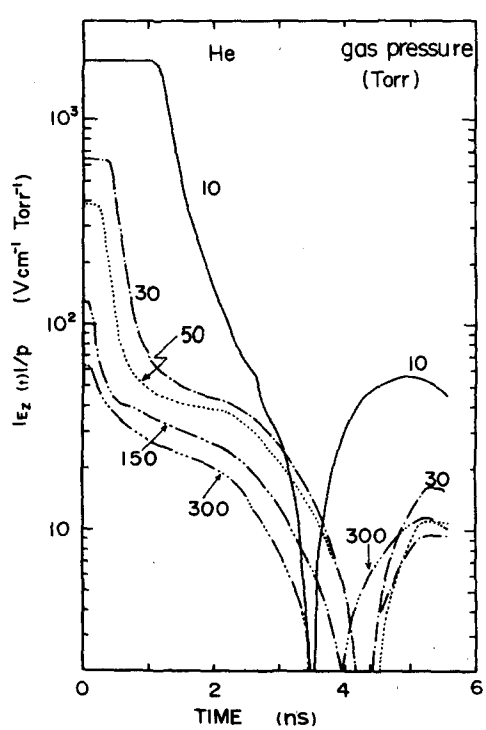

FIG. 10. The calculated $|E_z(t)|/p$ as a function of time for various pressures of He.

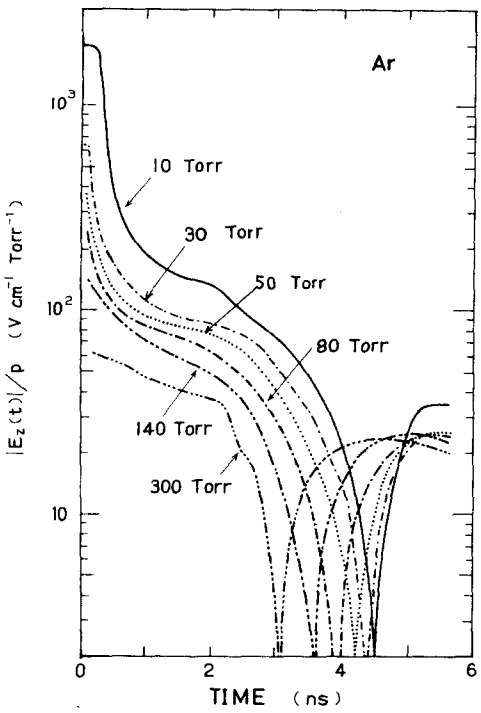

FIG. 11. The calculated $|E_z(t)|/p$ as a function of time for various pressures of Ar.

sensitively than $n_e(t)$. This is the reason why I_{back} decreases with increasing pressure. Of course, the variety of $Q_m(\bar{\epsilon})\epsilon^{1/2}$ among gases must be noticed.

When the values of D_{obs} at a certain pressure are compared among monatomic gases, according to the above analysis, the larger I_{net} or the smaller I_{back} streams in the gas giving the larger D_{obs}. Since the larger I_{net} induces the larger E_z in Eq. (1), the larger D_{obs} at the fixed pressure indicates the larger E/p despite of the smaller I_{back}. From Eq. (4), I_{back} or $\sigma_e E_z$ is proportional to the product of $n_e(t)/Q_m(\bar{\epsilon})\bar{\epsilon}^{1/2}$ and E/p. Therefore, $n_e(t)$ must be the smaller for the gas giving the larger D_{obs} if $Q_m(\bar{\epsilon})\bar{\epsilon}^{1/2}$ is assumed to be almost the same among these gases. Since the number density of secondary electrons produced by direct ionization is only 4.5×10^{13} cm^{-3} at 50 Torr of He or at 10 Torr of Ar, the value of $n_e(t)$ is mostly produced by secondary ionization by E_z (electron avalaching). Then, in Eq. (2), $n_e(t)$ is determined mainly by the second term, $n_e(t)/t_i(t)$ in the pressure region in which D_{obs} increases gradually with pressure. Consequently, the larger value of t_i results in the larger D_{obs}.

From Eq. (3), pt_i can be expressed by

$$1/(pt_i) = w(\alpha/p - \eta/p) \; ; \tag{11}$$

when $\eta = 0$ as in monatomic gases,

$$1/(pt_i) = w\alpha/p \; . \tag{12}$$

Values of w and α/p are known as functions of E/p for various gases.[12,13] Since these data have been measured under steady-state conditions, they may not be applied directly to the electron beam with the ns pulse duration. However, they can be used as the measure of those parameters for such a beam.

For monatomic gases, the magnitudes of w for E/p below 100 Vcm^{-1} Torr^{-1} are in the order[12,13]

$$\text{He} \approx \text{Ne} > \text{Ar} \approx \text{Kr} \approx \text{Xe} \; , \tag{13}$$

and those of α/p for E/p below 80 Vcm^{-1} Torr^{-1} are in the order

$$\text{Ne} > \text{He} \approx \text{Ar} \approx \text{Kr} > \text{Xe} \; . \tag{14}$$

Then, the magnitude of $w\alpha/p$ has the following order:

$$\text{Ne} > \text{He} > \text{Ar} \approx \text{Kr} > \text{Xe} \; . \tag{15}$$

Therefore, at the fixed pressure at which $E/p < 100$ Vcm^{-1} Torr^{-1}, the order of t_i should be inverse to the above order (15). From Figs. 10 and 11, the value of E/p is supposed to be less than 100 Vcm^{-1} Torr^{-1} for all the monatomic gases at pressures above 70 Torr. On the other hand, the values of D_{obs} at pressures above 70 Torr in Fig. 9 are in the order

$$\text{Ne} < \text{He} < \text{Ar} < \text{Kr} \; , \tag{16}$$

as predicted from the order (15). Data on D_{obs} for Xe cannot be obtained at pressure above 30 Torr due to multiple scattering of the beam by Xe.[1] Values of $Q_m(\bar{\epsilon})\bar{\epsilon}^{1/2}$ in Eq. (4) for He and Ne are about one-eighth of those for Ar and Kr. Then, the values of D_{obs} become smaller for He and Ne than those expected from t_i. The values of D_{obs} at pressures below 50 Torr are smaller for Ar than for He in Fig. 9. This may be due to the larger value of α/p for Ar than for He at E/p above 80 Vcm^{-1} Torr^{-1}.[12]

On the other hand, pt_i can be also expressed as

$$\frac{1}{n_0 t_i} = \left(\frac{2}{m}\right)^{1/2} \int_{IP}^{\infty} \epsilon^{1/2} \sigma_{ion}(\epsilon) F(\epsilon) \, d\epsilon \; , \tag{17}$$

where IP is the ionization potential of a gas and $F(\epsilon)$ the distribution function for secondary electrons with energy ϵ. Data on σ_{ion} for lower-energy electrons have been measured for various gases by Rapp and Englander-Golden.[13,14] The heavier monatomic gas gives the lower IP and the larger σ_{ion}. Therefore, in order to give the larger t_i for the heavier gas as concluded from the order (16), the larger part of secondary electrons must have ϵ lower than the IP. In fact, the values of $\bar{\epsilon}$ used for the present computation are lower than IP as described already.

ACKNOWLEDGMENTS

The authors wish to express their thanks to Sin-ichi Sato and Minoru Maeda of Fujitsu Ltd., in Computing Center, Tokai Research Establishment, JAERI, for their valuable advice and help in programming and computation.

[1] H. Hotta and H. Arai, J. Chem. Phys. 67, 3608 (1977).
[2] F. F. Rieke and W. Prepejchal, Phys. Rev. A 6, 1507 (1972).
[3] C. C. Ling, H. Weiss, and E. R. Epp, Radiat. Res. 56, 307 (1973).
[4] P. Felsenthal and J. M. Proud, Phys. Rev. Sect. A 139, 1796 (1965).
[5] D. A. McArthur and J. W. Poukey, Phys. Rev. Lett. 27, 1765

(1971); Phys. Fluids **16**, 1996 (1973).
[6]D. W. Swain, J. Appl. Phys. **43**, 396 (1972).
[7]I. M. Kapchinskij and V. V. Vladimirskij, Proceedings of the International Conference on High Energy Accelerators and Instrumentation, 274, CERN Scientific Information Service, Geneva (1959).
[8]H. Arai and H. Hotta, Radiat. Res. **77**, 405 (1979).
[9]C. S. Lakshiminarasimha and J. Lucas, J. Phys. D **10**, 313 (1977).
[10]A. L. Gilardini, *Low Energy Electron Collisions in Gases* (Wiley-Interscience, New York, 1971).
[11]H. H. Landolt and R. Börnstein, *Zahlenwerte und Funktionen* (Springer, Berlin, 1956), Vol. 1, Pt. 1.
[12]J. Dutton, J. Phys. Chem. Ref. Data **4**, 577 (1975).
[13]L. G. Christophorou, *Atomic and Molecular Radiation Physics* (Wiley-Interscience, New York, 1972).
[14]D. Rapp and P. Englander-Golden, J. Chem. Phys. **43**, 1464 (1975).